2D-3D CNN based architectures for spectral reconstruction from RGB images

Sriharsha Koundinya[*,1,2] , Himanshu Sharma[*,1], Manoj Sharma[*,1], Avinash Upadhyay[*,1],
Raunak Manekar[1], Rudrabha Mukhopadhyay[1], Abhijit Karmakar[1,2], Santanu Chaudhury[1,2]
[1]CSIR-CEERI, [2]AcSIR
Pilani, Rajasthan 333031.
{sriharsharaja, himanshusharma102, mksnith, avinres,
raunakmanekar38, rudrabha, abhijit.karmakar, schaudhury} @gmail.com

Abstract

Hyperspectral cameras are used to preserve fine spectral details of scenes that are not captured by traditional RGB cameras that comprehensively quantizes radiance in RGB images. Spectral details provide additional information that improves the performance of numerous image based analytic applications, but due to high hyperspectral hardware cost and associated physical constraints, hyperspectral images are not easily available for further processing. Motivated by the performance of deep learning for various computer vision applications, we propose a 2D convolution neural network and a 3D convolution neural network based approaches for hyperspectral image reconstruction from RGB images. A 2D-CNN model primarily focuses on extracting spectral data by considering only spatial correlation of the channels in the image, while in 3D-CNN model the inter-channel co-relation is also exploited to refine the extraction of spectral data. Our 3D-CNN based architecture achieves very good performance in terms of MRAE and RMSE. In contrast to 3D-CNN, our 2D-CNN based architecture also achieves comparable performance with very less computational complexity.

1. Introduction

Hyperspectral imaging is a technique which captures numerous bands of electromagnetic wavelengths ranging from infrared spectrum to ultraviolet spectrum. Every matter has different spectral characteristics, capturing the differences in these characteristics can be of critical importance in a wide variety of applications like medical imaging [12] [31][36], remote sensing [6][7][9][27][38] and forensics[19]. Hyperspectral images capture the details of the scene by sensing multiple narrow band intensities. The additional spectral information embedded in hyperspectral data has enabled the use of hyperspectral images for various applications in computer vision tasks i.e recognition [40][39][44], tracking [24][41], document analysis and pedestrian detection [19][23]. It has also been used in applications such as geosensing [32], food [45] and other image analysis. Though hyperspectral imaging is highly advantageous, the cameras are very costly to manufacture. This creates a bottleneck for low-cost consumer applications. Further hyperspectral imaging requires high spectral resolution, it also needs more exposure time to create a noiseless hyperspectral image[26].

The development of a simple, compact and cost-effective system is limited by conventional hyperspectral imaging systems. These hyperspectral systems usually depend on the use of an imaging spectrograph, a mechanical filter or a liquid crystal filter. A spectrometer-free imaging system is required to build an affordable and compact system for hyperspectral imaging to spread its utilization. To implement these types of systems, it would require an algorithm which can effectively regenerate complete spectral information from RGB image. Various methods have been explored for spectral reconstruction from RGB data [10][35][33][29].

1.1. Related Work

Hyperspectral images are used in remote sensing application for more than three decades [17]. NASA's AVIRIS[18] uses hyperspectral imaging systems which acquire images by using 'whisk broom' scanning method. In this method, set of mirrors and fiber optics are used to redirect the incoming light to a bank of spectrometers. Recent systems use the 'push broom' scanning strategy [20] in which, hyperspectral image is obtained in a line-by-line manner by using optical elements and light sensitive (i.e. CCD) sensors. Some applications such as medical imaging uses tuneable or interchangeable narrow band filters [28] [37] to collect spectral data. However, hyperspectral images with the spatial and temporal resolution with special-

* Authors contributed equally

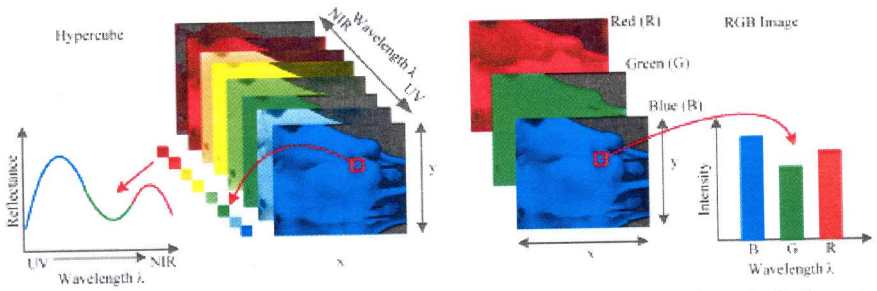

Figure 1. Comparison between RGB image and hypercube. Hypercube contains 3-dimensional data of a 2-dimensional image which are captured on each wavelength The left most represent the spectral signature.The right most represents the RGB image intensity curve for each pixel. Image reproduced from [26]

ized hardware based strategies is not physically possible. So various methods have been proposed to get fast and accurate hyperspectral images.

Computed tomography imaging spectrometers (CTIS)[11] [21] is used to construct 3D hyperspectral data from 2D imaging sensor. The hyperspectral image can be constructed by using multiplexed 2D data, but post processing and specialized hardware are required as a whole to perform the operation. Due to sensor size limitation the quality of hyperspectral images suffers in terms of spatial and spectral resolution. Recent advancement in the field of compressed sensing enhances the performance of CTIS in term of sensor utilization[8] [15] however, complex acquisition and significant post processing still remains bottleneck. Systems such as "Hyperspectral fovea" [13] etc. which are capable of acquiring high resolution RGB data, along with the spectral information of the central image region in the image, are also proposed which acquire real time hyperspectral images without causing much computational costs. These systems are mostly used in applications where occasional hyperspectral sampling area are required rather than full hyperspectral cube. Matrix factorization [22] method is used to construct hyperspectral data with high resolution with the help of RGB image and spectral images of low resolution. This methods produce high estimation accuracy with high computation cost. Recent literature [**?**] [14] [16] [30] in hyperspectral shows the researcher are estimating spectral values by using color images(RGB).In recent years deep learning techniques have given effective and reliable performance for solving non-linear problems. However, extraction of hyperspectral data from image using deep learning has not been explored extensively. The available literature [1] [14][2][42] showed success of deep learning in constructing high resolution hyperspectral images with simply using color images and their corresponding low resolution spectral images. In this paper, motivated by the potential of convolutional neural network (CNN) based architectures in [1] [42][2], which achieve on-par performance with state of art, we present 2D and 3D CNN architectures for reconstruction of spectral data from RGB images. In [2] spectral reconstruction has been done using generative adversarial network. In CNN, features are extracted from the image by convolving kernels on the image, these kernels are updated using various optimizers to construct the required features. In this paper, we explore application of both 2D and 3D kernels for spectral reconstruction from RGB image. A detailed comparison of the results obtained from application of these kernels is also given. In the next section we will describe the problem of reconstructing spectral image from RGB images.

2. Proposed Framework

2.1. Problem formulation

In basic color science the conventional color images are formed by 3 channels i.e Red , Blue and Green which have a strong dependency on the characteristics of imaging system that include the illuminance for image acquisition. Unlike color images, spectral reflectance is proven to be the most accurate representation of the color of an object and it is also completely independent of the imaging system. As shown in Figure 1 hyperspectral image generally covers a common portion of visible spectrum with numerous spectral bands and higher spectral resolution than three-band imaging (such as RGB images).

The mapping between a hyperspectral reflectance spectrum and an RGB reflectance spectrum [25] for each pixel at (x, y) can be modeled as[10] [35],

$$\mu_{3\times1} = S_{3\times N} * r_{N\times1} + e_{3\times1} \tag{1}$$

where μ is a 3×1 vector that has RGB intensities, S is a $3 \times N$ matrix of spectral responses of the three-color camera sensor, r is an $N \times 1$ vector that has the reflectance intensity normalized by the reflectance standard, and e is a 3×1 vector of system noise with zero mean. N represents the

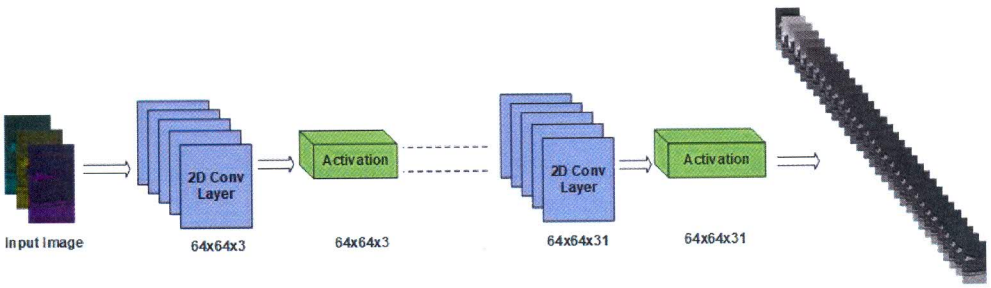

Figure 2. 2D-CNN proposed architecture

number of wavelengths. In general, S is obtained from the sensor manufacturer or it can be estimated analytically by training RGB samples [5] [34].

The goal is to predict r, reflectance vector, provided S and μ using equation 1. Please note that equation 1 belongs to a system of linear equations and the dimension of S is $3 \times N$, so there exists an infinite number of solutions which satisfy equation 1.

Let us suppose, a color spectrum μ and respective reflectance spectrum r is collected for every sample, $X_{m\times 3}$ and $\hat{R}_{m\times N}$ can be formed by organizing the spectra from numerous independent samples, where N is the number of wavelength and m is the number of dissimilar samples. The problem of reconstruction is supposed to learn conversion matrix T from the training set such that

$$\hat{R}_{n\times N} = X_{m\times 3} * T_{3\times N} \tag{2}$$

Relative absolute error can be used to compute T by minimizing error between reconstructed spectra and original spectra. After computing T using training set, (reflectance spectrum) can be estimated by using a RGB spectrum X as testing set.

The above formulation views the spectral reconstruction from RGB images a linear problem. The frameworks used in this work maps the nonlinear function from 3 channel RGB to 31 channel hyperspectral image.

$$Y_{n\times N} = F(X_{m\times 3}) \tag{3}$$

where F is a non linear mapping between X and Y and $Y \approx \hat{R}$. Two frameworks have been proposed in this paper based on its kernel type. The first framework has 2D convolutional kernels and the second has 3D convolutional kernels. The models are trained to extract the frequency based information from the image. The last layer of the models have 31 feature maps with every feature map having $10nm$ difference in wavelength from the consecutive feature. The input to these models are RGB images which have wavelength between $400nm$ to $700nm$ and the ground truth have thirty one images having wavelength starting from $400nm$ to $700nm$ with every image at $10nm$ step. 2D-CNN model as shown in Figure 2, having 2D kernel extracts the hyperspectral information available in the spatial domain of the specific channel. The kernel convolves on individual channels and the average of the values generated for each pixel on these channels are considered. This technique efficiently incorporates the spatial data however, an inter-channel co-relation is left unnoticed and holds important information. To incorporate the inter-channel co-relation we use 3D-CNN as shown in Figure 3 with 3D kernel. A 3D kernel convolves in three dimensions, two spatial and one channel, hence incorporates the related information between the channels. Instead of simply averaging a 3D convolution operation adds up the response of all the corresponding pixels, thus incorporating the correlated information.

2.2. 2D-CNN

Representation of RGB to hyperspectral conversion using 2D-CNN is explained as follows:

Let X be the RGB input of dimension $L \times H \times 3$ and Y be the ground truth hyperspectral image of dimension $L \times H \times 31$, Here L is the length, H is height/width and 3 or 31 is channels. Input X is represented as $C \times L \times H$. where C represent channel.

Feature Extraction: Feature extraction from input X is given by

$$X_1 = F_1(X) = max(0, X * W_1 + B_1) \tag{4}$$

Here W_1 contains n_1 filters of size $C \times f_1 \times f_1$ and B_1 is n_1-dimensional vector.

The dimension of x_1 is $n_1 \times L \times H$, $'*'$ is 2D convolution operator.

Non-Linear Mapping

$$X_2 = F_2(X_1) = max(0, X_1 * W_2 + B_2) \tag{5}$$

Here W_2 contains n_2 filters of size $n_1 \times f_2 \times f_2$ and B_2 is n_2 dimension vector. The dimension of X_2 is $n_2 \times L \times H$

$$X_{L-1} = F_{L-1}(X_{L-2}) = max(0, X_{L-2} * W_{L-1} + B_{L-1}) \tag{6}$$

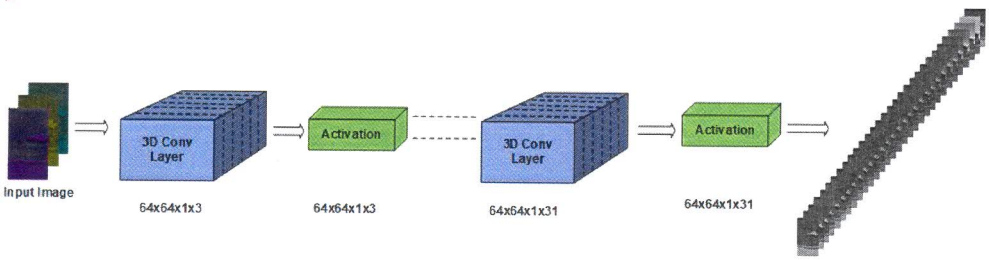

Figure 3. 3D-CNN proposed architecture

Reconstruction: Reconstruction of hyperspectral images is given by

$$X_L = F_L(X_{L-1}) = max(0, X_{L-1} * W_L + B_L) \quad (7)$$

Here W_L is 31 filters of size $f_L \times f_L$ and B_2 is 31 dimension vector. The dimension of X_L will be $31 \times L \times H$ now the loss can be calculated by

$$loss = ||Y - X_L||_2^2 \quad (8)$$

and we back propagate the gradient of loss to update the weight and bias in each epoch.

2.3. 3D-CNN

We treat channels as depth by considering channel (c) = 1 and depth(d) = 3. Mathematical formulation of RGB to hyperspectral conversion using 3D-CNN is modeled as follows:

Let X be represented as of dimension $c \times d \times L \times H$ or $1 \times d \times L \times H$ or $d \times L \times H$

Feature Extraction: Feature extraction from input X is given by

$$X_1 = \mathcal{F}_1(X) = max(0, X \otimes W_1 + B_1) \quad (9)$$

Here $\mathcal{F}$ represents the operation by a 3D kernel '$\otimes$' is 3D convolution operator and W_1 contains n_1 filters of size $d_1 x f_1 x f_1$ or $1 \times d_1 \times f_1 \times f_1$, Here ($\because d_1 < d$)

The dimension of X_1 will be $n_1 \times L \times H$.

Non-linear Mapping in Multiple Steps :

$$X_2 = \mathcal{F}_2(X_1) = max(0, X_1 \otimes W_2 + B_2) \quad (10)$$

Here W_2 contain n_2 filter of size $d_2 \times f_2 \times f_2$ ($\because d_2 < n_1$)

$$X_{L-1} = \mathcal{F}_{L-1}(X_{L12}) \quad (11)$$

Hence W_{L-1} contains n_{L-1} filter of size $d_{L-1} \times f_{L-1} \times fL - 1$ ($\because d_{L-1} \leq n_{L-2}$)

Reconstruction:

Reconstruction of hyperspectral images given by

$$X_L = \mathcal{F}_L(X_{L-1}) = X_{L-1} \otimes W_L + B_L \quad (12)$$

Here W_L is 31 filter of size $d_L \times f_L \times f_L$ ($\because d_L \leq n_{L-1}$) The dimension X_L will be $31 \times L \times H$ Same the loss is calculated as by equation 3 and similarly the weights are update by back propagating the gradient loss.

2.4. Training

Individual models have been trained on distinct datasets [4][3][43]. We extracted the patches of size $64 \times 64 \times 3$ from RGB input images and patches of size $64 \times 64 \times 31$ are extracted from corresponding hyperspectral image. For NTIRE challenge, total number of training patches are 84021. We trained a 5-layer architectures for both 2D and 3D CNN with learning rate of 10^{-4} with different hyper parameters. For training 3D-CNN, the channels of the RGB image is considered as depth. To create such dataset, we split the channels of RGB and reshaped them in $(height, width, 1)$ format followed by concatenating these channels along third axis. This creates the data with the shape $(height, width, 1, channels)$. Similar approach is followed to create corresponding ground truth. Patches of size 64×64 are then extracted from this dataset. This data is then passed to the model as explained section 2.3 and section 2.4. The kernel size for both the models are 3×3 and $3 \times 3 \times 3$ respectively. CNN performs exceptionally well for non-linear problems, however selection of trainable parameters is quite a tedious task. The parameters are chosen using brute force cracking. Parameters giving optimum results with less complexity are considered. To train the model we are using Adam optimizer and minimizing the mean absolute error between the model output and ground truth.

2.5. Testing

To test the model, learned model is inferred. Testing can be represented for both 2D-CNN and 3D-CNN model by.

$$\begin{aligned} X_L &= G_L(X_{L-1}) \\ &= G_L(F_{L-1}(X_{L-2})) \\ &= G_L.F_{L-1}.....F_1(X) \\ \because X_L &= G(X) \end{aligned} \quad (13)$$

where G represents both F and $\mathcal{F}$.

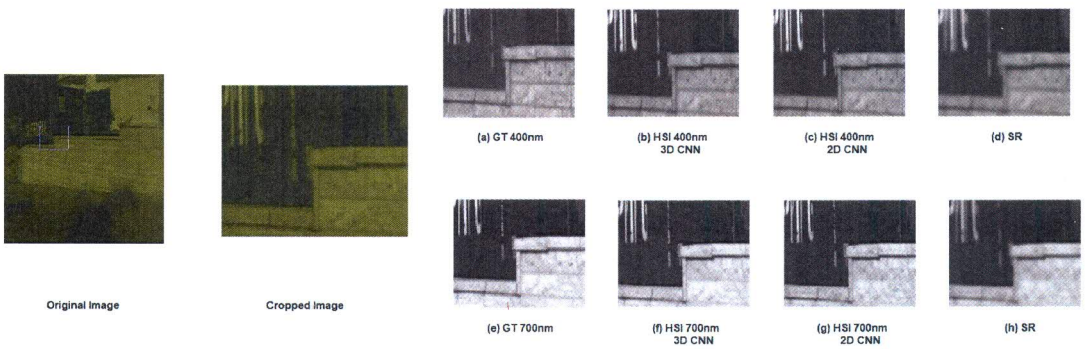

Figure 4. Hyperspectral image comparison on NTIRE-2018 dataset

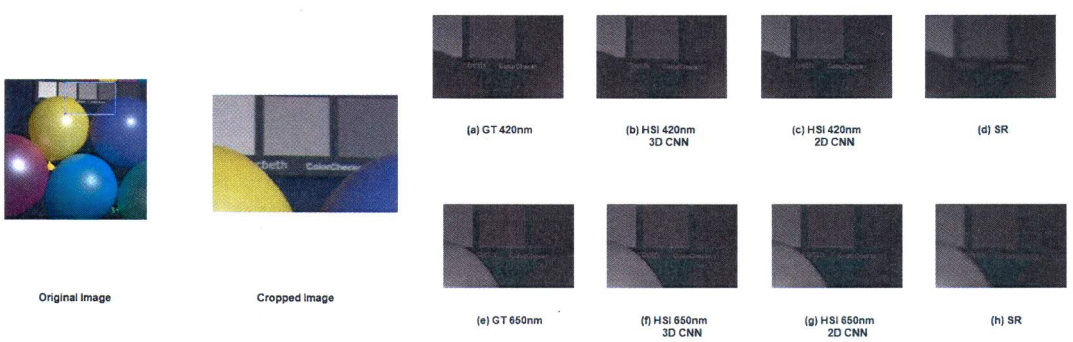

Figure 5. Hyperspectral image comparison on CAVE dataset

3. Experimental Results

We implemented our algorithms using Keras and Tensorflow, running on Intel Core i7 CPU at 3.6 GHz with 16 GB RAM and Nvidia 8 GB GTX 1080 GPU. We evaluated the proposed approach using the hyperspectral images from NTIRE-2018[4], iCVL[3] and CAVE [43] databases. Root Mean Square Error (RMSE), Mean Squared error(MSE) and Mean Relative Absolute Error (MRAE) are used as evaluation metrics. RMSE is useful in analyzing the reconstruction of individual spectral channels of the estimated hyperspectral images and MRAE is sensitive to extreme values (i.e outliers) and to low values.

3.1. Datasets

2D-3D CNN model are tested and trained using NTIRE-2018 image dataset[4], CAVE [43] and iCVL dataset [3]. NTIRE-2018 dataset consists of of 254 hyperspectral images captured by Specim PS Kappa DX4 camera with a rotary stage for the spatial scanning. Out of 256 hyperspectral images 201 images are taken from iCVL dataset [3]. The size of provided images are $1392 \times 1300 \times 31$ with 31 spectral channels in the range 400-700nm with 10nm steps. CAVE dataset consists 32 hyperspectral images taken by Apogee Alta U260 camera size of each image is512×512, it also consists of 31 spectral bands with range 400-700nm with 10nm steps.

The iCVL dataset consists of 202 images taken by Specim DX4 hyperspectral camera. Each image is of size $1392 \times 1300 \times 31$ spectral band images ranging from 400-700nm with 10nm steps.

3.2. Result Analysis

Table 1. Results on NTIRE-2018 dataset

Approach	RMSE	MRAE	Time (in seconds)
3D-CNN	**20.010**	**0.018**	**11**
2D-CNN	**21.394**	**0.020**	**2.3**
VIDAR[1]	14.45	0.0137	180
VIDAR[2]	13.98	0.0137	96
HypedPhoti	16.07	0.0153	57
LFB	16.19	0.0152	-
IVRL Prime	16.17	0.0155	170/2
sr402	16.92	0.0164	12
CVL	17.27	0.0174	1
adv$_rgb3hs$	24.81	0.0218	40
SPEC$_RC$	24.81	0.0401	-
sparse recovery(SR)[3]	24.03	0.056	-

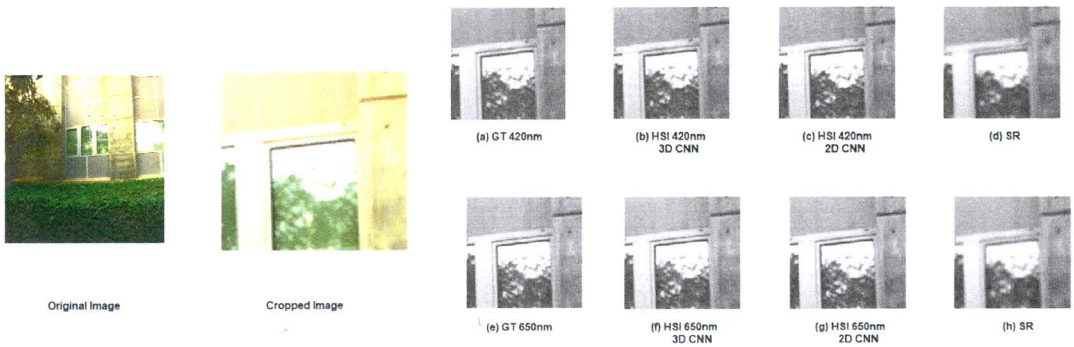

Figure 6. Hyperspectral image comparison on iCVL dataset

To illustrate the effectiveness of our proposed 2D & 3D CNN based approach to convert RGB to hyperspectral image, we have compared our techniques with other state-of-the-art methods(Table 1, Table 2, Table 3). For evaluating performance of our techniques we have used mean relative absolute error (MRAE), root mean square error (RMSE), mean squared error(MSE) and run time per image.

The results and comparison of methods from NTIRE-2018 challenge can be seen from Table 1. The proposed algorithms performs on par with other methods as can be observed by comparing RMSE and MRAE in both of the proposed methods with far less run time per image. We have also shown the relative performance of the proposed methods compared to other CNN based algorithms in Table 2 and Table 3 on CAVE and iCVL datasets respectively. As can be seen Figure 4 the 400nm band and also in 700nm band and Figure 5,Figure 6 for 420nm and 650 nm band 3D-CNN reconstruction has preserved finer details as compared to sparse recovery (SR). It is also evident from Figure 5,Figure 6 2D-CNN has also out performed sparse recovery (SR) method.

Table 2. Results on CAVE dataset

Approach	RMSE	MSE
3D-CNN	**2.86**	**0.0065**
2D-CNN	**3.05**	**0.0075**
S.R[3]	5.40	-
A+ 1×1[1]	2.74	-
A+ 3×3[1]	2.90	-

Table 3. Results on iCVL dataset

Approach	RMSE	MSE
3D-CNN	**1.115**	**0.0051**
2D-CNN	**2.12**	**0.0086**
alvarez et. al[2]	1.457	-
S.R[3]	2.56	-
A+ 1×1[1]	1.12	-
A+ 3×3[1]	1.04	-

4. Conclusion

We have given a CNN based framework to reconstruct multiple spectral bands (Hyperspectral image) from three spectral bands (RGB). Subsequently, we have shown that our CNN based deep learning model with minimal layer (5) have outperformed the current traditional method of extracting hyperspectral data from RGB images. It is also evident that our methods have very less run time requirement with the performance on par as compared to other methods presented in the challenge. We have compared 2D and 3D kernel based CNN for spectral reconstruction.

References

[1] J. Aeschbacher, J. Wu, R. Timofte, D. CVL, and E. ITET. In defense of shallow learned spectral reconstruction from rgb images. In *Proceedings of the IEEE Conference on Computer Vision and Pattern Recognition*, pages 471–479, 2017.

[2] A. Alvarez-Gila, J. van de Weijer, and E. Garrote. Adversarial networks for spatial context-aware spectral image reconstruction from rgb. *arXiv preprint arXiv:1709.00265*, 2017.

[3] B. Arad and O. Ben-Shahar. Sparse recovery of hyperspectral signal from natural rgb images. In *European Conference on Computer Vision*, pages 19–34. Springer, 2016.

[4] B. Arad, O. Ben-Shahar, R. Timofte, L. Van Gool, L. Zhang, M.-H. Yang, et al. Ntire 2018 challenge on spectral reconstruction from rgb images. In *The IEEE Conference on Computer Vision and Pattern Recognition (CVPR) Workshops*, June 2018.

[5] K. Barnard and B. Funt. Camera characterization for color research. *Color Research & Application*, 27(3):152–163, 2002.

[6] E. Belluco, M. Camuffo, S. Ferrari, L. Modenese, S. Silvestri, A. Marani, and M. Marani. Mapping salt-marsh vegetation by multispectral and hyperspectral remote sensing. *Remote sensing of environment*, 105(1):54–67, 2006.

[7] M. Borengasser, W. S. Hungate, and R. Watkins. *Hyperspectral remote sensing: principles and applications*. CRC press, 2007.

[8] D. J. Brady and M. E. Gehm. Compressive imaging spectrometers using coded apertures. In *Visual Information Processing XV*, volume 6246, page 62460A. International Society for Optics and Photonics, 2006.

[9] A. Castrodad, Z. Xing, J. Greer, E. Bosch, L. Carin, and G. Sapiro. Discriminative sparse representations in hyperspectral imagery. In *Image Processing (ICIP), 2010 17th IEEE International Conference on*, pages 1313–1316. IEEE, 2010.

[10] S. Chen and Q. Liu. Modified wiener estimation of diffuse reflectance spectra from rgb values by the synthesis of new colors for tissue measurements. *Journal of Biomedical optics*, 17(3):030501, 2012.

[11] M. Descour and E. Dereniak. Computed-tomography imaging spectrometer: experimental calibration and reconstruction results. *Applied Optics*, 34(22):4817–4826, 1995.

[12] D. T. Dicker, J. Lerner, P. Van Belle, D. Guerry, 4th, M. Herlyn, D. E. Elder, and W. S. El-Deiry. Differentiation of normal skin and melanoma using high resolution hyperspectral imaging. *Cancer biology & therapy*, 5(8):1033–1038, 2006.

[13] D. W. Fletcher-Holmes and A. R. Harvey. Real-time imaging with a hyperspectral fovea. *Journal of Optics A: Pure and Applied Optics*, 7(6):S298, 2005.

[14] S. Galliani, C. Lanaras, D. Marmanis, E. Baltsavias, and K. Schindler. Learned spectral super-resolution. *arXiv preprint arXiv:1703.09470*, 2017.

[15] M. Gehm, R. John, D. Brady, R. Willett, and T. Schulz. Single-shot compressive spectral imaging with a dual-disperser architecture. *Optics express*, 15(21):14013–14027, 2007.

[16] M. Goel, E. Whitmire, A. Mariakakis, T. S. Saponas, N. Joshi, D. Morris, B. Guenter, M. Gavriliu, G. Borriello, and S. N. Patel. Hypercam: hyperspectral imaging for ubiquitous computing applications. In *Proceedings of the 2015 ACM International Joint Conference on Pervasive and Ubiquitous Computing*, pages 145–156. ACM, 2015.

[17] A. F. Goetz, G. Vane, J. E. Solomon, and B. N. Rock. Imaging spectrometry for earth remote sensing. *Science*, 228(4704):1147–1153, 1985.

[18] R. O. Green, M. L. Eastwood, C. M. Sarture, T. G. Chrien, M. Aronsson, B. J. Chippendale, J. A. Faust, B. E. Pavri, C. J. Chovit, M. Solis, et al. Imaging spectroscopy and the airborne visible/infrared imaging spectrometer (aviris). *Remote sensing of environment*, 65(3):227–248, 1998.

[19] S. Hwang, J. Park, N. Kim, Y. Choi, and I. S. Kweon. Multispectral pedestrian detection: Benchmark dataset and baseline. *Integrated Comput.-Aided Eng*, 20:347–360, 2013.

[20] J. James. *Spectrograph design fundamentals*. Cambridge University Press, 2007.

[21] W. R. Johnson, D. W. Wilson, and G. Bearman. Spatial-spectral modulating snapshot hyperspectral imager. *Applied optics*, 45(9):1898–1908, 2006.

[22] R. Kawakami, Y. Matsushita, J. Wright, M. Ben-Ezra, Y.-W. Tai, and K. Ikeuchi. High-resolution hyperspectral imaging via matrix factorization. In *Computer Vision and Pattern Recognition (CVPR), 2011 IEEE Conference on*, pages 2329–2336. IEEE, 2011.

[23] Z. Khan, F. Shafait, and A. Mian. Automatic ink mismatch detection for forensic document analysis. *Pattern Recognition*, 48(11):3615–3626, 2015.

[24] S. J. Kim, F. Deng, and M. S. Brown. Visual enhancement of old documents with hyperspectral imaging. *Pattern Recognition*, 44(7):1461–1469, 2011.

[25] T. Kim, J.-I. Kim, M. A. V. Onufrak, C. Chapple, and Y. L. Kim. Nonspectroscopic imaging for quantitative chlorophyll sensing. *Journal of Biomedical Optics*, 21(1):016008, 2016.

[26] G. Lu and B. Fei. Medical hyperspectral imaging: a review. *Journal of biomedical optics*, 19(1):010901, 2014.

[27] F. Melgani and L. Bruzzone. Classification of hyperspectral remote sensing images with support vector machines. *IEEE Transactions on geoscience and remote sensing*, 42(8):1778–1790, 2004.

[28] P. J. Miller and C. C. Hoyt. Multispectral imaging with a liquid crystal tunable filter. In *Optics in Agriculture, Forestry, and Biological Processing*, volume 2345, pages 354–366. International Society for Optics and Photonics, 1995.

[29] R. M. Nguyen, D. K. Prasad, and M. S. Brown. Training-based spectral reconstruction from a single rgb image. In *European Conference on Computer Vision*, pages 186–201. Springer, 2014.

[30] M. Parmar, S. Lansel, and B. A. Wandell. Spatio-spectral reconstruction of the multispectral datacube using sparse recovery. In *Image Processing, 2008. ICIP 2008. 15th IEEE International Conference on*, pages 473–476. IEEE, 2008.

[31] L. L. Randeberg, I. Baarstad, T. Løke, P. Kaspersen, and L. O. Svaasand. Hyperspectral imaging of bruised skin. In *Photonic Therapeutics and Diagnostics II*, volume 6078, page 60780O. International Society for Optics and Photonics, 2006.

[32] R. Richter and D. Schläpfer. Geo-atmospheric processing of airborne imaging spectrometry data. part 2: atmospheric/topographic correction. *International Journal of Remote Sensing*, 23(13):2631–2649, 2002.

[33] A. Robles-Kelly. Single image spectral reconstruction for multimedia applications. In *Proceedings of the 23rd ACM international conference on Multimedia*, pages 251–260. ACM, 2015.

[34] H.-L. Shen and J. H. Xin. Spectral characterization of a color scanner by adaptive estimation. *JOSA A*, 21(7):1125–1130, 2004.

[35] H.-L. Shen, J. H. Xin, and S.-J. Shao. Improved reflectance reconstruction for multispectral imaging by combining different techniques. *Optics express*, 15(9):5531–5536, 2007.

[36] G. N. Stamatas, C. J. Balas, and N. Kollias. Hyperspectral image acquisition and analysis of skin. In *Spectral Imaging: Instrumentation, Applications, and Analysis II*, volume 4959, pages 77–83. International Society for Optics and Photonics, 2003.

[37] S. Tominaga. Multichannel vision system for estimating surface and illumination functions. *JOSA A*, 13(11):2163–2173, 1996.

[38] E. Underwood, S. Ustin, and D. DiPietro. Mapping nonnative plants using hyperspectral imagery. *Remote Sensing of Environment*, 86(2):150–161, 2003.

[39] M. Uzair, A. Mahmood, and A. Mian. Hyperspectral face recognition with spatiospectral information fusion and pls regression. *IEEE Transactions on Image Processing*, 24(3):1127–1137, 2015.

[40] M. Uzair, A. Mahmood, and A. S. Mian. Hyperspectral face recognition using 3d-dct and partial least squares. In *BMVC*, 2013.

[41] H. Van Nguyen, A. Banerjee, and R. Chellappa. Tracking via object reflectance using a hyperspectral video camera. In *Computer Vision and Pattern Recognition Workshops (CVPRW), 2010 IEEE Computer Society Conference on*, pages 44–51. IEEE, 2010.

[42] Z. Xiong, Z. Shi, H. Li, L. Wang, D. Liu, and F. Wu. Hscnn: Cnn-based hyperspectral image recovery from spectrally undersampled projections. In *Proceedings of the IEEE International Conference on Computer Vision Workshops*, volume 2, 2017.

[43] F. Yasuma, T. Mitsunaga, D. Iso, and S. K. Nayar. Generalized assorted pixel camera: postcapture control of resolution, dynamic range, and spectrum. *IEEE transactions on image processing*, 19(9):2241–2253, 2010.

[44] D. Zhang, W. Zuo, and F. Yue. A comparative study of palmprint recognition algorithms. *ACM computing surveys (CSUR)*, 44(1):2, 2012.

[45] Y. Zhao and R. S. Berns. Image-based spectral reflectance reconstruction using the matrix r method. *Color Research & Application*, 32(5):343–351, 2007.